MOLECULAR IMAGING AND BIOLOGY

Mol Imaging Biol (2017)
DOI: 10.1007/s11307-017-1093-7

RESEARCH ARTICLE

Characterization of Magneto-Endosymbionts as MRI Cell Labeling and Tracking Agents

Kimberly D. Brewer,[1,2] Ryan Spitler,[2] Kayla R. Lee,[3] Andrea C. Chan,[3] Joyce C. Barrozo,[3] Abdul Wakeel,[3] Chandler S. Foote,[3] Steven Machtaler,[2] James Rioux,[1,2] Juergen K. Willmann,[2] Papia Chakraborty,[3] Bradley W. Rice,[3] Christopher H. Contag,[2] Caleb B. Bell III,[3] Brian K. Rutt[2,4]

[1]*Biomedical Translational Imaging Centre (BIOTIC), Halifax, Nova Scotia, Canada*
[2]*Radiology Department and Molecular Imaging Program (MIPS), Stanford University, Stanford, CA, USA*
[3]*Bell Biosystems, San Francisco, CA, USA*
[4]*Richard M. Lucas Center for Imaging, Stanford University School of Medicine, The Lucas Expansion, Room PS-064, 1201 Welch Road, Stanford, CA, 94305-5488, USA*

Abstract

Purpose: Magneto-endosymbionts (MEs) show promise as living magnetic resonance imaging (MRI) contrast agents for *in vivo* cell tracking. Here we characterize the biomedical imaging properties of ME contrast agents, *in vitro* and *in vivo*.

Procedures: By adapting and engineering magnetotactic bacteria to the intracellular niche, we are creating magneto-endosymbionts (MEs) that offer advantages relative to passive iron-based contrast agents (superparamagnetic iron oxides, SPIOs) for cell tracking. This work presents a biomedical imaging characterization of MEs including: MRI transverse relaxivity (r_2) for MEs and ME-labeled cells (compared to a commercially available iron oxide nanoparticle); microscopic validation of labeling efficiency and subcellular locations; and *in vivo* imaging of a MDA-MB-231BR (231BR) human breast cancer cells in a mouse brain.

Results: At 7T, r_2 relaxivity of bare MEs was higher (250 s^{-1} mM^{-1}) than that of conventional SPIO (178 s^{-1} mM^{-1}). Optimized *in vitro* loading of MEs into 231BR cells yielded 1–4 pg iron/cell (compared to 5–10 pg iron/cell for conventional SPIO). r_2 relaxivity dropped by a factor of ~3 upon loading into cells, and was on the same order of magnitude for ME-loaded cells compared to SPIO-loaded cells. *In vivo,* ME-labeled cells exhibited strong MR contrast, allowing as few as 100 cells to be detected in mice using an optimized 3D SPGR gradient-echo sequence.

Conclusions: Our results demonstrate the potential of magneto-endosymbionts as living MR contrast agents. They have r_2 relaxivity values comparable to traditional iron oxide nanoparticle contrast agents, and provide strong MR contrast when loaded into cells and implanted in tissue.

Key words: Magnetic resonance imaging (MRI), Magnetotactic bacteria, Magnetite, Labeled cells, Iron, Cell tracking

Introduction

Superparamagnetic iron oxide (SPIO) contrast agents have been used for decades to track cells with magnetic resonance imaging (MRI) [1, 2]. MRI is the modality of choice for cell

Kimberly D. Brewer and Ryan Spitler contributed equally to this work.

Correspondence to: Brian Rutt; *e-mail:* brutt@stanford.edu

Published online: 14 June 2017

tracking due to its non-invasive nature, 3D imaging capabilities and full anatomic access, but requires addition of a contrast agent to discriminate transplanted from resident cells in tissue [3]. Previous work has shown that it is possible to achieve *in vivo* single cell detection and visualization of cells labeled with SPIOs using MRI [4]. Using this extreme sensitivity, MRI has enabled the tracking of metastases originating from single cells [5]. MRI has also been used to track cell migration to direct cell therapies for different diseases, including dendritic and cytotoxic T cell therapies used for treatment of cancer [6].

SPIO particles used for cell tracking span a wide range of sizes and coatings [7]; however, in all cases they are static, passive, synthetic particles with a small number of iron oxide crystals at the core (in some cases, a single crystal). SPIO-based cell tracking agents have a few limitations that have prevented more widespread usage. *In vivo,* through apoptosis or exocytosis, SPIOs can label tissue or phagocytic cell types resulting in false positive signals not representative of the target cells; in other words, SPIOs lack live cell specificity [8]. In rapidly dividing cell types, the concentration decreases as cells divide, leading to eventual loss of signal which limits longitudinal studies.

Reporter gene approaches utilize a signal-generating mechanism such as a protein (*i.e.,* the reporter) that overcomes dilution issues and typically only produces signal when the cells are viable. As cells proliferate, the genes continue to express the reporter, resulting in a persistent cell tracking capability. Furthermore, a reduction in signal indicates reduced viability while absence of signal indicates cell death. Reporter genes have been used extensively for optical (both fluorescence and bioluminescence) and positron emission tomography (PET) molecular imaging [9, 10]; however, use of optical cell tracking techniques can be limited in larger animals due to tissue penetration restrictions and genetic engineering requirements, and are thus not easily translated to human uses. PET and single-photon emission computed tomography (SPECT) are quite sensitive and do not have penetration limitations; however, the requirement for radioactivity raises safety requirements, increases costs, and has limited widespread use, especially for longitudinal studies [11]. Additionally, PET and SPECT have limited spatial resolution and radionuclide decay makes long-term cell tracking studies more challenging.

Several groups have developed MR reporter genes aiming to increase intrinsic iron uptake in cells under genetic control [12–14]; however, only limited success has been demonstrated to date, likely due to the intrinsic complexity of magnetic phenotypes in nature. Research into iron-based MR reporter genes has primarily focused on two main types: (1) overexpression of ferritin, transferrin, or other iron storage or transport genes [12, 15–19], and (2) expression of genes originating from magnetotactic bacteria [20–22]. While both types of reporter genes have seen some success in animal models, widespread adoption remains elusive. These difficulties stem from the inability to generate sufficient quantities of iron loading per cell leading to poor contrast and inability to detect small numbers of cells.

As mentioned above, magnetotactic bacteria have been identified as a potential source for transgenes, and this has been an active research area. These bacteria coordinate over 100 genes to generate magnetosomes (multiple magnetite particles arranged in linear chain-like structures, with each magnetite particle encapsulated within a lipid bilayer) that generate the magnetic phenotype. Because of the large number of genes necessary, classic genetic approaches may be insufficient to transfer this phenotype from prokaryotic to eukaryotic systems [23]. Simpler MR reporters based on one or two magnetotactic bacterial genes have been proposed but have not met with much success.

An alternative which our group is pursuing [24] follows the endosymbiotic theory of organelle biogenesis and uses the entire magnetotactic bacterium as the cell tracking agent. Aside from producing strong MR contrast changes due to their magnetosomal content, magnetotactic bacteria have the potential to self-replicate, making them interesting candidates for longitudinal studies. Synchronized propagation within host cells as in the case of the endosymbiotic organelles (mitochondria, plastids, *etc.*) is the ultimate goal and recent studies demonstrated feasibility of this [25]. Even without synchronization, MEs present a significant advantage over traditional contrast agents for *in vivo* cell tracking. Upon host cell death, conventional SPIOs are often taken up by other cell types, resulting in false positives [8, 26–30], whereas we have found that the signal from magnetotactic bacterial constructs loaded into mammalian cells is more completely and rapidly cleared upon cell death [24].

The application of magnetotactic bacteria as MR contrast agents has been reported [31]; in this case, *Magnetospirillum magneticum* strain AMB-1 bacteria were directly injected intravenously. Owing to their anaerobic or microaerophilic nature, these bacteria preferentially migrate to hypoxic tumors [31]. This prior literature provides proof-of-principle that magnetotactic bacteria can be effective as MR contrast agents. Here, we propose a safer use of these bacteria, by labeling mammalian cell populations with whole magnetotactic bacteria *in vitro*, injecting or implanting these mammalian cells, and then following these cells *in vivo* by MRI. Once bacteria are taken up into mammalian cells, we refer to them generically as *magneto-endosymbionts* or MEs. Owing to their intracellular compartmentalization, MEs have reduced contact with the recipient animal system, making their use safe for preclinical studies and classified as biosafety level 1 [24].

In this work, we define various preclinical biomedical imaging properties of MEs, dissect the subcellular processing post labeling, and show their potential as novel MR contrast agents for direct cell labeling and tracking. We measured the MR transverse relaxivity (r_2) behavior of bare MEs, cell loading efficiency, and MR relaxivity of loaded cells, in comparison to a commercially available SPIO, Molday ION. In addition, we probed the detection sensitivity

of ME-labeled cells in a mouse model by direct intracranial injections followed by *in vivo* and postmortem imaging.

Materials and Methods

ME Preparation

MEs (trade name Magnelles®), were obtained from Bell Biosystems, Inc. (San Francisco, CA) and handled per manufacturer guidelines.

Eukaryotic Cell Labeling

As a representative mammalian cell, commonly used in other cell tracking literature, we used MDA-MB-231BR, a human breast adenocarcinoma cell line that preferentially metastasizes in the brains of intra-cardiac injected mice. The 231BR cell line was maintained in Dulbecco's modified Eagle's medium (DMEM) containing 10 % FBS and 1 % penicillin/streptomycin at 37 °C and 5 % CO_2. The cells were labeled with either MEs (Bell Biosystems, Inc. San Francisco, CA), or Molday ION Rhodamine B SPIO particles (BioPAL, Worcester, MA). ME-labeling was conducted according to manufacturer-provided guidelines; however, concentrations of up to 10,000 MPC (MEs per cell) were used in some cases [24]. For Molday labeling, cells were incubated with 25 µg/ml of the iron nanoparticles for approximately 18 h. All labeled cells were washed three times with 1X PBS prior to characterization or *in vivo* imaging. Cell viability was assessed using Trypan blue staining, and labeling efficiency was assessed using confocal microscopy.

Microscopy

For confocal microscopy, cells were grown overnight on poly-L-lysine coated coverslips. MEs were visualized by fluorescence microscopy using an ME-specific antibody to cell surface proteins [32], and an anti-rabbit Alexa 546 secondary antibody (Invitrogen). Molday particles come tagged with a Rhodamine B fluorescent marker by the manufacturer. Cells were also stained with DAPI and phalloidin (633 nm, Invitrogen) for improved intracellular localization of MEs or Molday particles. Confocal microscopy was performed on a Zeiss LSM710 Imager (Carl Zeiss Canada Ltd., Canada).

Iron Characterization

Both ME and ME-labeled mammalian cell iron loading levels were measured using inductively coupled plasma optical emission spectrometry (ICP-OES). To prepare samples for ICP-OES, 750 µl of concentrated nitric acid was added to samples for digestion of organic material. Samples were transferred to glass tubes and kept overnight in a hot oil bath at ~130 °C. Samples were then diluted with 2 % nitric acid and iron measurements were made with a Thermo ICAP 6300 Duo View Spectrometer (Thermo Fisher Scientific, Waltham MA).

MTS Assay

Cell proliferation was measured using the MTS (3(4,5-dimethylthiazol-2-yl)-5(3-car-boxymethoxyphenyl)-2-(4-sulfophenyl)-2H–tetrazolium) proliferation assay (CellTiter 96® Aqueous Non-Radioactive Cell Proliferation Assay; Promega, Madison, Wisconsin) according to the manufacturer's instructions. 5×10^4, 1×10^5, or 2×10^5 ME-labeled or unlabeled cells were seeded in 100 µl of media in triplicate in individual wells of a flat-bottom 96-well plate. Cells were incubated overnight at 37 °C with 5 % CO_2. The MTS dye was added directly to the cell culture media and incubated for 1 h at 37 °C and the absorbance was then measured at 490 nm.

Sample Preparation

For characterization of relaxivity properties, all samples were prepared by suspending various concentrations of MEs, Molday particles or labeled cells in 200 µl of Matrigel (Corning, Tewksbury MA). These samples were stored in mini-PCR tubes for imaging on a 7T MRI scanner. All samples were vortexed and quickly set in a 37 °C water bath to ensure homogeneous distribution of particles within the Matrigel.

MR Relaxation Characterization

*r*2 relaxivity was measured for both MEs and Molday particles as well as labeled 231BR cells, at a field strength of 7T. These measurements were acquired using a GE Discovery MR950 7T MRI system (General Electric Healthcare, Waukesha, WI). A single-channel receive-only coil was used around the sample, with excitation performed by a larger transmit-only volume coil that produced uniform radiofrequency excitation of the small sample. T_2 measurements were made using a 16-echo spin-echo sequence with TR = 3000 ms and echo spacing =6.6 ms. T_2 relaxation times were derived on a voxel-by-voxel basis by single-exponential non-linear least squares fitting using Matlab (The Mathworks, Natick, MA); mean T_2 values for the sample were then derived from the resulting T_2 map by averaging voxels within a central cross-section through the sample tube.

Relaxation times were converted to relaxation rates, *e.g.*, $R_2 = 1/T_2$. Relaxivity (r_2) was calculated as the slope of the linear relationship between R_2 and total iron concentration as determined by ICP-OES. We report relaxivities using ICP-

OES-measured total iron to be consistent with prior literature; however, it should be noted that this underestimates ME relaxivity, because there is a substantial amount of iron present throughout the bacteria that is not in magnetosomal form, and does not produce MRI contrast. This issue is discussed in greater detail elsewhere. All data are displayed as mean ± standard error.

Animal Model

A total of four female foxn1 Nu/nu mice, 6–8 weeks old (Charles River Laboratories, Wilmington, MA, USA) were used and cared for in accordance to the guidelines of both the National Institutes of Health and Stanford University.

To evaluate the ability of MRI to detect small numbers of labeled cells, an intracranial injection model with decreasing numbers of cells was used. Cells were injected *via* direct intracranial injection. Mice were anesthetized and a small portion of the skull was removed slightly over the midline. For one mouse each, either 10^2 or 10^3 ME-labeled cells were suspended in 5 µl of Matrigel and injected into the cerebral cortex just right of midline, with the same number of unlabeled cells being injected into the contralateral cortex as negative controls. Additionally, 10^2 Molday-labeled cells were injected into one mouse as a positive control. Bone glue was used to patch the hole in the skull to prevent leakage of cells. Mice were immediately imaged *in vivo* using MRI, and were sacrificed immediately following MRI. These experiments were intended as pilot experiments to bracket the range of ME-labeled cells that could be detected, and not intended for statistical analysis; for this reason, single animals were used.

In Vivo Imaging

All *in vivo* MRI imaging was performed on a 7T GE-Agilent Discovery MR901 MRI system (General Electric Healthcare, Waukesha, WI). Mice were imaged using an optimized 3D SPGR gradient-echo sequence. Imaging parameters for the SPGR sequence were: 150 µm isotropic resolution, TR/TE = 30/3.7 ms, flip angle =20°, and four averages. All images were viewed and analyzed using the OsiriX software package [33]. Further image analysis was performed for the mice receiving 10^2 and 10^3 labeled cells. Using RView software [34], ROIs were drawn on the control side (where injected cells contained no iron, such that the hypointensity was due only to the needle track) and on the labeled cell side (where injected cells contained iron label, such that hypointensity was due to both iron and the needle track). We then calculated the minimum signal intensity within each hypointense region, and computed the percent signal intensity decrease on the labeled cell side compared to the unlabeled cell side, for each labeled cell type. Comparison of signal intensity between labeled and control cell injections was deemed to be a more direct and reliable method to measure the effect of the ME- and Molday-loaded cells *versus* using correlative histology, which is particularly challenging in the case of such small numbers of injected cells.

Statistical Analysis

A one-way analysis of variance (ANOVA) was performed to test for statistically significant differences using the SPSS statistics software package (IBM Corp., Armonk, NY); $p < 0.05$ was considered to be significant.

Results

Characterization of ME-Labeled Cells In Vitro

The ability of MEs to be taken up in sufficient quantities by eukaryotic 231BR cancer cells was initially verified using immunocytochemistry (Fig. 1a, b). Confocal microscopy images demonstrated that MEs were present inside labeled cells, and in some cases it was possible to visualize the spiral shape of individual MEs within a cell. Both MEs and Molday appeared to be clustered in the perinuclear region of the cell.

Labeling cells with MEs and Molday particles did not appear to affect cellular viability, with both types of labeled 231BR cells exhibiting >90 % viability *via* Trypan blue exclusion, consistent with other experiences with ME or Molday labeling [24, 35, 36]. An MTS assay was used to assess cellular proliferation of ME-labeled 231BR cells, and no changes in proliferation were observed due to the presence of MEs (Fig. 2).

Total iron load per ME (as quantified by ICP-OES) was found to be in the range of 10 fg Fe/ME. The average cell loading for Molday was 6.6 pg/cell, with standard deviation 2.7 pg/cell. The average cell loading for MEs was 4.1 pg/cell, with standard deviation 0.8 pg/cell. These total iron values were used for relaxivity calculations.

Transverse (r_2) relaxivity measurements for MEs and Molday particles were found to be 250.2 ± 9.0 s^{-1} mM^{-1} for bare MEs in Matrigel, relative to 177.9 ± 2.2 s^{-1} mM^{-1} for bare Molday particles in Matrigel (Fig. 3a); the higher value of r_2 for MEs compared to Molday was statistically significant ($p < 0.01$). In Fig. 3b, r_2 relaxivities for ME- and Molday-labeled 231BR cells are shown. As a result of cell compartmentalization, r_2 relaxivity decreased substantially compared to the corresponding bare particles. r_2 values for ME- and Molday-labeled 231BR cells were 35.4 ± 0.5 s^{-1} mM^{-1} and 61.9 ± 1.0 s^{-1} mM^{-1}, respectively. In this case, the lower value of r_2 for ME-labeled compared to Molday-labeled cells was statistically significantly ($p < 0.01$).

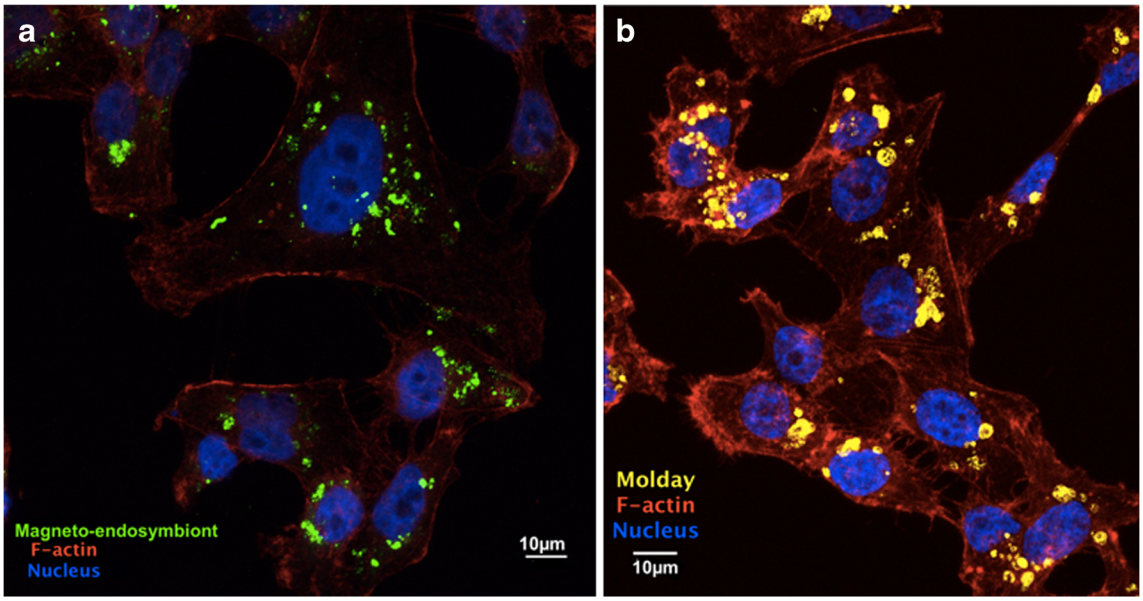

Fig. 1. Confocal fluorescence microcopy of cell labeling IHC and viability of MDA-MB-231BR cells. These labeled eukaryotic cells readily take up MEs as shown (MEs present inside of labeled cells). Once taken up, both particles types, MEs and Molday appear to be clustered in the perinuclear region of the cell. IHC of ME **a**, **b** Molday-labeled MDA-MB-231BR cells with MEs (*green*), Molday (*yellow*), F-acting (*red*) and nuclei (*blue*).

Characterization of ME-Labeled Cells In Vivo

ME-labeled cell injections of 10^3 and 10^2 cells, as well as the Molday-labeled cell injection of 10^2 cells, were detectable *in vivo* at 7T (Fig. 4). The injection of 10^3 ME-labeled cells caused an 86 % reduction in signal intensity compared to that produced by the injection of unlabeled cells. The injection of 10^2 ME-labeled cells caused a 32 % reduction in signal intensity compared to control injection; by comparison, the injection of 10^2 Molday-labeled cells caused an 18 % drop in normalized signal intensity compared to control injection. We conclude from these results that ME-labeling produces a similar detectability as Molday labeling, and that the threshold of detectability for ME-labeled cells is definitely less than 1000 cells and possibly less than 100 cells.

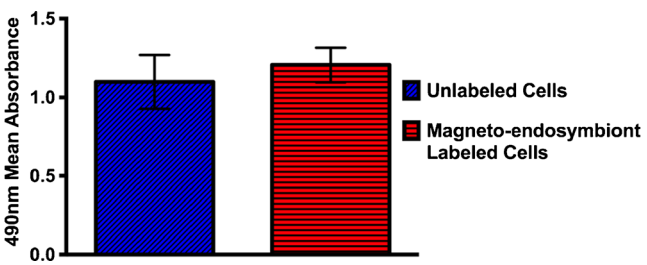

Fig. 2. The MTS viability results comparing ME-labeled and unlabeled cells. Cells were loaded with MTS dye using a 96-well plate format and the absorbance was then measured at 490 nm. No statistically significant changes in cellular proliferation were observed in labeled MDA-MB-231BR cells in the presence of MEs compared to unlabeled cells. Therefore, the MTS assay indicated labeling cells with MEs did not affect cell viability or proliferation.

Discussion

In this study, MEs were validated as a preclinical MRI contrast agent for cell labeling and tracking. We measured and compared r_2 relaxivity values for MEs and commercially available Molday ION Rhodamine B, a conventional SPIO MR contrast agent.

Similar to most other conventional SPIO contrast agents, Molday particles consist of iron oxide cores surrounded by an organic coating (total hydrodynamic size 35 nm). However, MEs consist of multiple magnetite particles, each of diameter >30 nm, arranged typically in linear chain-like structures. Each magnetite particle is encapsulated within a lipid bilayer (constituting the magnetosome), which is further encapsulated within the bacterial cell itself (see [32] for representative transmission electron microscopy images).

Transverse relaxivity (r_2) is the most relevant parameter for characterizing iron-based cell tracking agents, since most research studies use either T_2 or T_2* weighted contrast for *in vivo* imaging. We found that r_2 values for bare MEs were significantly *higher* than those of Molday particles, indicating that MEs are intrinsically very strong MR contrast agents. Our measured r_2 relaxivity for MEs (250 s^{-1} mM^{-1} at 7T) is consistent with work by Meriaux et al. [37], who found the r_2 relaxivity of purified AMB-1 magnetosomes to be 489 s^{-1} mM^{-1} at 17.2T (a higher r_2 value for purified magnetosomes is expected as some level of bacterial cell

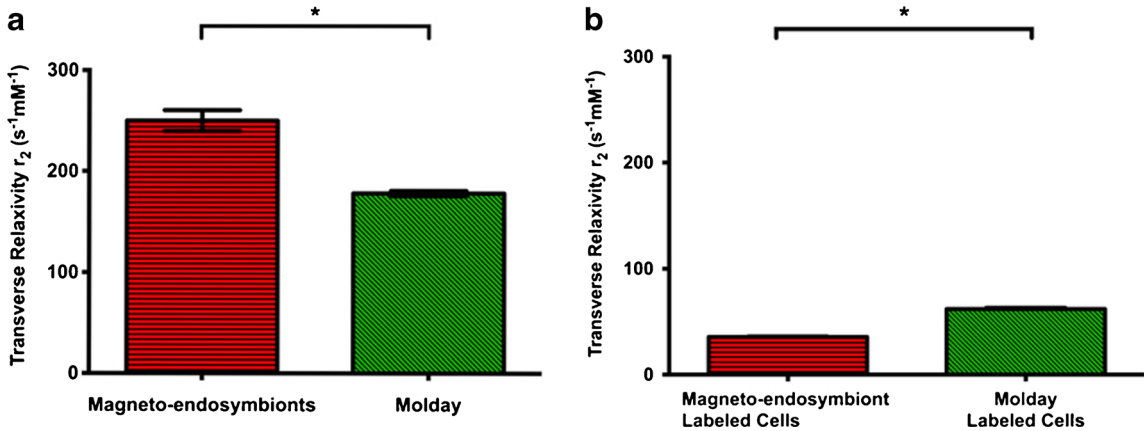

Fig. 3. Comparison of ME and Molday transverse relaxivities of both bare particles in Matrigel and labeled MDA-MB-231BR cells in Matrigel. **a** r_2 relaxivity of MEs and Molday alone and **b** ME and Molday-labeled MDA-MB-231BR cells at 7T. Measurements were made using a 16-echo spin-echo sequence with TR = 3000 ms and echo spacing = 6.6 ms and mean T_2 values for the sample were then derived from the resulting T_2 map by averaging voxels within a central cross-section through the sample tube. Relaxation times were converted to relaxation rates (*plotted*), and normalized to iron concentration. (A single asterisk indicates statistical significance of $p < 0.01$).

compartmentalization has been eliminated). Our measured r_2 relaxivity for Molday particles of 178 s^{-1} mM^{-1} is in line with previous observations [37, 38]. The increased r_2 relaxivity for MEs compared to Molday particles is likely due to the differences in size, shape, crystal structure, and coating of magnetosomes in comparison to Molday. It should be noted that the measured r_2 relaxivity of iron oxide particles depends on the echo spacing used in the multi-echo spin-echo pulse sequence [39, 40], and this echo spacing has not been well standardized in the

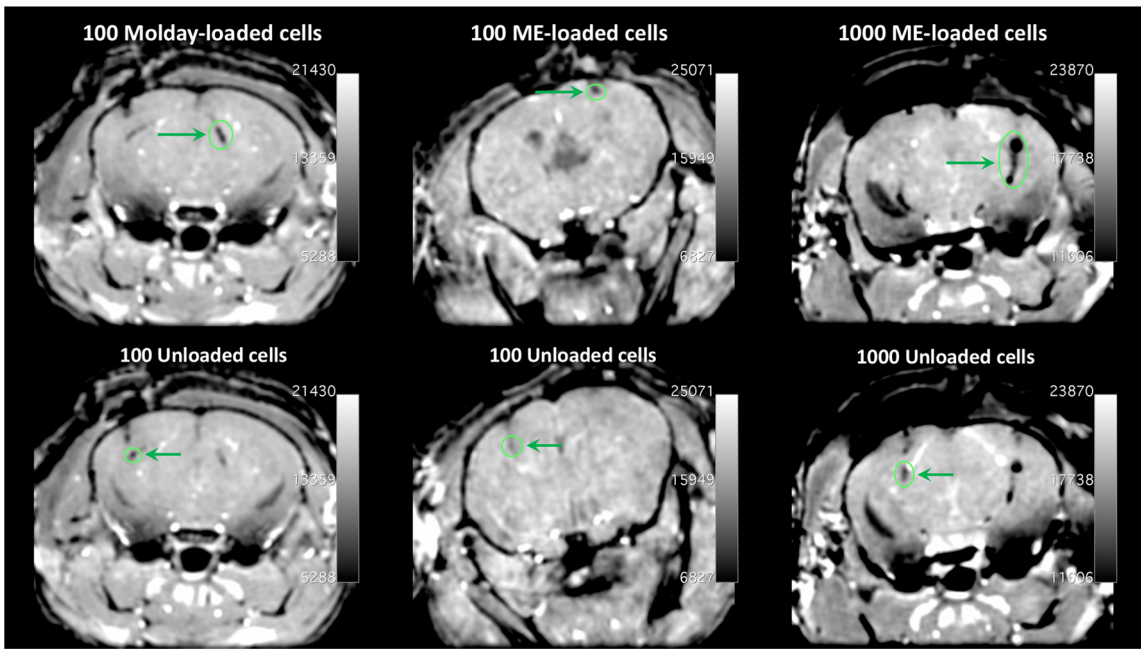

Fig. 4. *In vivo* MRI detection of Molday-labeled compared to ME-labeled MDA-MB-231BR cells. Labeled cells and unlabeled cells were injected intracranially as indicated, with labeled cells injected on the right side (*top row*) and unlabeled cells injected on the contralateral side (*bottom row*). Injected cell numbers were: 10^2 Molday-labeled cells (*left column*), 10^2 ME-labeled cells (*middle column*), and 10^3 ME-labeled cells (*right column*). Images were acquired using an optimized 3D SPGR gradient-echo sequence: 150 μm isotropic resolution, TR/TE = 30/3.7 ms, flip angle =20°, four averages. All images were viewed and analyzed using the OsiriX software package. The slice showing minimum signal intensity consistent with the injection track is displayed and an ROI placed around the minimum signal region; within that ROI, minimum signal was recorded. Percent decrease in this minimum signal for labeled cell region *versus* unlabeled cell region was used as the quantitative metric of labeled cell effect.

literature. We used 6.6 ms for our 7T measurements, which was close to that used by Meriaux et al.; on the other hand, other publications have used echo spacing values as high as 24 ms [38].

Because of the biological nature of MEs, there is a substantial amount of naturally occurring iron within bacterial cells apart from that found in magnetosomes; however, only the magnetosomal iron generates MRI contrast. Therefore, any measure of total iron (*e.g.,* from ICP-OES) will not accurately represent the contrast producing iron in MEs. In this paper, we calculated relaxivity by dividing the relaxation rate by total iron concentration, in keeping with literature convention; however, the contrast producing magnetosomes within MEs only make up approximately 30 % of the total iron [32]. So, by normalizing to a higher amount of iron we are in fact underestimating the relaxivity of MEs.

In addition to characterizing the r_2 relaxivity of MEs, we evaluated the ability to load eukaryotic cells with MEs, confirming iron loading levels using ICP-OES. These results indicate sufficient relaxivity and loading levels for MRI detection. The ME-labeling protocol was first optimized to maximize relaxivity per eukaryotic cell (cell R_2), which is the property most directly linked to MRI-based detection limits. For 231BR cells, the final optimized protocol was a ratio of 8500 MEs per cell (MPC) and an incubation time of ~18 h. The MPC of 8500 was selected because this was the highest ratio that did not produce observable toxicity or adverse changes to cells. The 18 h incubation was optimal logistically, however shorter incubations are possible. Incubations as short as 1.5 h have been used, producing similar though inferior cell tagging efficiency (data not shown).

The MTS assay indicated that labeling cells with MEs did not affect cell viability or proliferation. Confocal fluorescent images (as seen in Fig. 1) demonstrate intracellular localization of MEs within 231BR cells. The MEs appear to be clustered in the perinuclear region of cells, similar to Molday particles. While some individual MEs with the typical spiral shape are visible in these images, many appear to be in a more spherical morphology. This could arise for at least three reasons: the ME are not coplanar with the field of view, the MEs are stressed (which can result in a cocci shape) [41], or the MEs may be contained within a vesicle (*i.e.,* endosomes), as is the case for Molday particles.

We found that the r_2 relaxivity for ME-labeled cells (35 s^{-1} mM^{-1}) was much lower than for MEs alone (250 s^{-1} mM^{-1}), corresponding to a reduction of ~86 %. This was a larger percent drop than exhibited by Molday-labeled cells, whose relaxivity of 62 s^{-1} mM^{-1} corresponded to a drop of ~65 % compared to 178 s^{-1} mM^{-1} measured for Molday alone. The larger percent decrease in relaxivity for ME-labeled cells may be due to the additional layers of compartmentalization for MEs relative to Molday, which is expected to cause a larger restriction of water access to the iron cores. Reductions of r_2 relaxivity upon cellular compartmentalization by similarly high percentages has been reported in prior literature [38]. Again by normalizing to total iron, we are also overestimating the contrast producing iron fraction and getting a lower *r*2.

Based on the drop in r_2 relaxivity seen in labeled cells compared to bare particles, we can surmise that both MEs and Molday-labeled cells are in the static dephasing regime (see [42, 43] for discussion of this theory and its application to iron-loaded cells). By the same static dephasing regime theory, this decrease in r_2 relaxivity should be accompanied by an *increase* in r_2* relaxivity upon cellular compartmentalization, resulting in an increase in T_2* contrast in appropriately weighted images.

In addition to *in vitro* characterization, we also evaluated the MEs by characterizing their detection sensitivity *in vivo* to determine their utility for cell tracking. We attempted to bracket the range of cell detectability by directly injecting two different numbers of labeled cells into the brain—100 and 1000—(with an equal number of unlabeled cells placed contralaterally as a control). As seen in Fig. 4 as well as the quantitative measurements of relative signal intensity drop, as few as 100 ME-labeled cells were detectable using a T_2* weighted spoiled gradient-echo pulse sequence at 7T; this detectability was similar to that seen for Molday-labeled cells. This demonstrated that, despite the decreased r_2 compared to Molday-labeled cells, there was still a significant amount of T_2* contrast (as predicted by static dephasing regime theory), allowing even a small number of ME-labeled cells to generate sufficient contrast for detection. These results provide preliminary evidence for comparable detection sensitivity for ME-labeled cells compared to Molday-labeled cells. More extensive experiments that are beyond the scope of this proof-of-concept study will be necessary to characterize the limit of detectability for ME-labeled cells in greater detail.

One key area that will require additional development is the replication of the ME within the host cell. The elucidation of the longer term longitudinal fate of MEs inside cells is still a work in progress. It is known that MEs are digested through the autophagy pathway [32]. However using ME-labeled cardiomyocytes which do not divide, injected into the myocardium of mice, labeled cells could be detected for up to 14 days [24]; indicating that the contrast producing magnetosome is stable after ME digestion. In cells capable of dividing, such as cancer cells, magnetosomes will dilute over time and cells will eventually drop below the detection threshold. MEs have been shown to reproduce and transfer themselves to progeny cells using a direct cytosolic introduction approach and a cell type where autophagy is suppressed [32]. However, in typical cell types where autophagy is active, ME tracking agents are eventually degraded through the autophagocytosis pathway [32]. Further elucidation of autophagy in relation to MEs symbiosis is underway, and will include the study of mechanisms employed by natural intracellular prokaryotes.

Finally, in terms of safety and translatability, while the agent itself represents a living bacteria, previous studies have demonstrated that even intravenous injection of large numbers of magnetotactic bacteria (10^9) alone do not show signs of organ toxicity or an immune response in immune-competent rats [24]. The intracellular fate of MEs is addressed in [32] in the short-time range, whereas a recent publication by Mahmoudi et al. shows data on the intracellular fate of MEs for up to 14 days in non-dividing cells [24]. The latter publications contains additional data on safety and toxicity, and [32] discusses the process of autophagy that is the principal cause of ME digestion as well as the retention of magnetosomes after autophagy. This data is encouraging with regard to the possible translational impact of this platform, especially when considering that the MEs are further shielded from the injected host's immune system as a result of their being loading into cells prior to injection for cell tracking applications. Additional experiments to assess the host immune response to ME-labeled cells, and to investigate the influence of chemo or radiation therapy on the fate of this novel living contrast agent, are planned. In summary, we believe that MEs will be a useful preclinical tool for the investigation of both fundamental biological mechanisms and diseases.

Conclusion

Our studies show that MEs have potential for use as novel magnetite-based MR contrast agents for cell tracking. MEs demonstrate r_2 relaxivity values comparable to traditional iron oxide nanoparticle contrast agents, and demonstrate strong MR contrast when loaded into cells. As few as 100 ME-labeled 231BR cells could be detected *in vivo* using a commonly available 7T MRI protocol, demonstrating that MEs could be used for a wide range of cell tracking needs. Further exploration and characterization of the relaxivity properties of MEs and their longer term behavior in cells, could help direct the optimization and application of this novel class of MRI cell-labeling probe.

Acknowledgements. The authors would like to acknowledge technical assistance from Adam Shuhendler, Marjan Rafat, Edward Graves, and Rehan Ali, and the support from the following funding sources: NIH SBIR Phase I 1R43TR001202-01, CIRM RT2-02018, and NIH T32-CA-009695.

Compliance with Ethical Standards

Conflict of Interest

Ryan Spitler was a consultant for Bell Biosystems Inc. Kayla R. Lee, Andrea C. Chan, Joyce C. Barrozo, Abdul Wakeel, Chandler S. Foote, Papia Chakraborty and Bradley W. Rice were all employed by Bell Biosystems during this work. Christopher H. Contag serves on the scientific advisory board of Bell Biosystems. Caleb B. Bell III is the CEO of Bell Biosystems.

References

1. Li L, Jiang W, Luo K et al (2013) Superparamagnetic iron oxide nanoparticles as MRI contrast agents for non-invasive stem cell labeling and tracking. Theranostics 3:595–615
2. Schlorf T, Meincke M, Kossel E et al (2010) Biological properties of iron oxide nanoparticles for cellular and molecular magnetic resonance imaging. Int J Mol Sci 12:12–23
3. Bulte JW (2009) *In vivo* MRI cell tracking: clinical studies. Am J Roentgenol 193:314–325
4. Foster-Gareau P, Heyn C, Alejski A, Rutt BK (2003) Imaging single mammalian cells with a 1.5 T clinical MRI scanner. Magn Reson Med 49:968–971
5. Heyn C, Ronald JA, Ramadan SS et al (2006) *In vivo* MRI of cancer cell fate at the single-cell level in a mouse model of breast cancer metastasis to the brain. Magn Reson Med 56:1001–1010
6. Ahrens ET, Bulte JW (2013) Tracking immune cells *in vivo* using magnetic resonance imaging. Nat Rev Immunol 13:755–763
7. Roohi F, Lohrke J, Ide A et al (2012) Studying the effect of particle size and coating type on the blood kinetics of superparamagnetic iron oxide nanoparticles. Int J Nanomedicine 7:4447–4458
8. Bernau K, Lewis CM, Petelinsek AM et al (2016) *In vivo* tracking of human neural progenitor cells in the rat brain using magnetic resonance imaging is not enhanced by ferritin expression. Cell Transplant 25:575–592
9. Cevenini L, Calabretta MM, Calabria D et al (2015) Luciferase genes as reporter reactions: how to use them in molecular biology? Adv Biochem Eng Biotechnol 154:3–17
10. Youn H, Chung JK (2013) Reporter gene imaging. Am J Roentgenol 201:W206–W214
11. Naumova AV, Modo M, Moore A et al (2014) Clinical imaging in regenerative medicine. Nat Biotechnol 32:804–818
12. Pereira SM, Moss D, Williams SR et al (2015) Overexpression of the MRI reporter genes ferritin and transferrin receptor affect iron homeostasis and produce limited contrast in mesenchymal stem cells. Int J Mol Sci 16:15481–15496
13. Vandsburger MH, Radoul M, Cohen B, Neeman M (2013) MRI reporter genes: applications for imaging of cell survival, proliferation, migration and differentiation. NMR Biomed 26:872–884
14. Vande Velde G, Himmelreich U, Neeman M (2013) Reporter gene approaches for mapping cell fate decisions by MRI: promises and pitfalls. Contrast Media Mol Imaging 8:424–431
15. Patrick PS, Rodrigues TB, Kettunen MI et al (2016) Development of Timd2 as a reporter gene for MRI. Magn Reson Med 75:1697–1707
16. Naumova AV, Yarnykh VL, Balu N et al (2012) Quantification of MRI signal of transgenic grafts overexpressing ferritin in murine myocardial infarcts. NMR Biomed 25:1187–1195
17. Naumova AV, Reinecke H, Yarnykh V et al (2010) Ferritin overexpression for noninvasive magnetic resonance imaging-based tracking of stem cells transplanted into the heart. Mol Imaging 9:201–210
18. He X, Cai J, Liu B et al (2015) Cellular magnetic resonance imaging contrast generated by the ferritin heavy chain genetic reporter under the control of a Tet-On switch. Stem Cell Res Ther 6:207
19. Pereira SM, Herrmann A, Moss D et al (2016) Evaluating the effectiveness of transferrin receptor-1 (TfR1) as a magnetic resonance reporter gene. Contrast Media Mol Imaging 11:236–244
20. Zhang XY, Robledo BN, Harris SS, Hu XP (2014) A bacterial gene, mms6, as a new reporter gene for magnetic resonance imaging of mammalian cells. Mol Imaging 13:2–12
21. Goldhawk DE, Gelman N, Sengupta A, Prato FS (2015) The interface between iron metabolism and gene-based iron contrast for MRI. Magn Reson Insights 8(Suppl 1):9–14
22. Zurkiya O, Chan AW, Hu X (2008) MagA is sufficient for producing magnetic nanoparticles in mammalian cells, making it an MRI reporter. Magn Reson Med 59:1225–1231
23. Yan L, Zhang S, Chen P et al (2012) Magnetotactic bacteria, magnetosomes and their application. Microbiol Res 167:507–519
24. Mahmoudi M, Tachibana A, Goldstone AB et al (2016) Novel MRI contrast agent from magnetotactic bacteria enables *in vivo* tracking of iPSC-derived cardiomyocytes. Sci Rep 6:26960
25. Agapakis CM, Niederholtmeyer H, Noche RR et al (2011) Towards a synthetic chloroplast. PLoS One 6(4):e18877

26. Amsalem Y, Mardor Y, Feinberg MS et al (2007) Iron-oxide labeling and outcome of transplanted mesenchymal stem cells in the infarcted myocardium. Circulation 116(Suppl):I38–I45
27. Berman SC, Galpoththawela C, Gilad AA et al (2011) Long-term MR cell tracking of neural stem cells grafted in immunocompetent versus immunodeficient mice reveals distinct differences in contrast between live and dead cells. Magn Reson Med 65:564–574
28. Srivastava AK, Bulte JW (2014) Seeing stem cells at work *in vivo*. Stem Cell Rev 10:127–144
29. Guenoun J, Ruggiero A, Doeswijk G et al (2013) *In vivo* quantitative assessment of cell viability of gadolinium or iron-labeled cells using MRI and bioluminescence imaging. Contrast Media Mol Imaging 8:165–174
30. Nguyen PK, Riegler J, Wu JC (2014) Stem cell imaging: from bench to bedside. Cell Stem Cell 14:431–444
31. Benoit MR, Mayer D, Barak Y et al (2009) Visualizing implanted tumors in mice with magnetic resonance imaging using magnetotactic bacteria. Clin Cancer Res 15:5170–5177
32. Lee KR, Wakeel A, Chakraborty P et al (2017) Cell labeling with magneto-endosymbionts and the dissection of the subcellular location, fate and host cell interactions. Molecular Imaging and Biology. doi:10.1007/s11307-017-1094-6
33. Rosset A, Spadola L, Ratib O (2004) OsiriX: an open-source software for navigating in multidimensional DICOM images. J Digit Imaging 17:205–216
34. Studholme C (2016) RView Software, Version #9.043B
35. Khurana A, Nejadnik H, Chapelin F et al (2013) Ferumoxytol: a new, clinically applicable label for stem-cell tracking in arthritic joints with MRI. Nanomedicine (Lond) 8:1969–1983
36. Shen WB, Plachez C, Chan A et al (2013) Human neural progenitor cells retain viability, phenotype, proliferation, and lineage differentiation when labeled with a novel iron oxide nanoparticle, Molday ION Rhodamine B. Int J Nanomedicine 8:4593–4600
37. Meriaux S, Boucher M, Marty B et al (2015) Magnetosomes, biogenic magnetic nanomaterials for brain molecular imaging with 17.2 T MRI scanner. Adv Healthc Mater 4:1076–1083
38. Taylor A, Herrmann A, Moss D et al (2014) Assessing the efficacy of nano- and micro-sized magnetic particles as contrast agents for MRI cell tracking. PLoS One 9:e100259
39. Rozenman Y, Zou XM, Kantor HL (1990) Cardiovascular MR imaging with iron oxide particles: utility of a superparamagnetic contrast agent and the role of diffusion in signal loss. Radiology 175:655–659
40. Ghugre NR, Coates TD, Nelson MD, Wood JC (2005) Mechanisms of tissue-iron relaxivity: nuclear magnetic resonance studies of human liver biopsy specimens. Magn Reson Med 54:1185–1193
41. Lefevre CT, Bazylinski DA (2013) Ecology, diversity, and evolution of magnetotactic bacteria. Microbiol Mol Biol Rev 77:497–526
42. Yablonskiy DA, Haacke EM (1994) Theory of NMR signal behavior in magnetically inhomogeneous tissues: the static dephasing regime. Magn Reson Med 32:749–763
43. Bowen CV, Zhang X, Saab G et al (2002) Application of the static dephasing regime theory to superparamagnetic iron-oxide loaded cells. Magn Reson Med 48:52–61